






# Towards Multiscale Neural Operator Framework of Accretion and Feedback Applications

Nihaal Bhojwani <sup>δ,1,2</sup> Chuwei Wang (王楚惟) <sup>δ</sup> <sup>1</sup> Hai-Yang Wang (王海洋) <sup>δ</sup> <sup>3,4</sup> Chang Sun (孙畅) <sup>5</sup> Elias R. Most <sup>3,4</sup> and Anima Anandkumar <sup>1</sup>

<sup>1</sup>*Computing and Mathematical Sciences, California Institute of Technology, CA 91125, USA*

<sup>2</sup>*Department of Computer Sciences, University of Maryland*

<sup>3</sup>*TAPIR, California Institute of Technology, Pasadena, CA 91125, USA*

<sup>4</sup>*Walter Burke Institute for Theoretical Physics, California Institute of Technology, Pasadena, CA 91125, USA*

<sup>5</sup>*Department of Physics, California Institute of Technology, Pasadena, CA 91125, USA*

We present the method combining neural operator (NO) and direct **[multi-level]** numerical simulations for accretion and feedback problem, in both magnetohydrodynamic (MHD) and general relativistic magnetohydrodynamic (GRMHD) simulations. NO is trained to learn the semigroup of the numerical simulation at small scale and provide the boundary condition for the next level of simulation. As a first step towards multiscale simulations, we focus on black hole feeding and feedback problem. **[Findings:]** This method is generally applicable as the subgrid model of all the central accretor problems.

## I. INTRODUCTION

**[HYW: Multiscale problems.]** Numerical simulations in astrophysics enables us to investigate a broad range of highly complex problems. Yet many longstanding questions persist because these systems are intrinsically multiscale in both space and time. Systems with a central accretor—such as the coevolution of supermassive black holes (SMBH) and their host galaxies, star and planet formation, and stellar-mass black holes or neutron stars in supernova remnants—are canonical examples of such multiscale phenomena.

Among all these multiscale problems, feeding and feedback of the SMBHs attracted a lot of attentions. The SMBHs harbored at the centers of most galaxy nuclei play a crucial role in the evolution of the galaxies, shown in various properties such as stellar and dark matter bulge masses **[Needs citation]**. Ideally one needs to resolve the small-scale dynamics near the event horizon (mpc size), while simultaneously resolving the large-scale dynamics of the host galaxy (kpc to Mpc size), making this a formidable task for direct numerical simulations. Consequently, the accretion flows around SMBHs and their feedbacks are modelled typically by a subgrid model in cosmological simulation **[Needs citation]**. And the accretion and outflow dynamics near the black hole are often modeled by general relativistic magnetohydrodynamic simulations (GRMHD). Due to the ignorance of accretion disk formation history, a torus in hydrodynamic equilibrium is usually adopted as the idealized initial condition [1]. Early attempt to bridge the feeding problem and construct a more realistic black hole accretion problem includes modelling infall and accretion from the Bondi radius [2].

**[HYW: Relativistic outflows.]** The feedback from low-Eddington accreting black holes are carried out mainly

through relativistic outflows (winds and jets) **[Needs citation]**. Especially, the jets are observed from AU to Mpc scales, far beyond the range of host galaxies. These relativistic outflows can efficiently deposit energy and momentum into the interstellar medium (ISM) and intergalactic medium (IGM), triggering large-scale turbulence, and thus affect the star formation and galaxy evolution **[Needs citation]**.

**[HYW: Black hole feeding and feedback problem.]** **[HYW: And Computational advances.]** A considerable amount of efforts adopting various techniques has been made to bridge different scales, which includes direct simulation assuming smaller scale separation [3–6], “zoom-in” adopting nested mesh in grid codes [7, 8], and “Lagrangian hyper-refinement” in Lagrangian codes [9, 10], remapping between different simulations, and “multi-zone” [11–13] or “cyclic-zoom” [14] methods iteratively refining and de-refining the simulation domain near the central black hole. Earlier attempts on bridging scales adopting “two-zone” techniques have been made in the content of hydrodynamic accretion [15].

**[HYW: Spatial-Temporal multiscale variability problem.]** Except the direct simulation modifying the scale separation, only the “multi-zone” and “cyclic-zoom” methods are able to capture feedback from the small-scale and evolve the different domains to convergence. These two methods are very similar, but different in details, particularly the treatment on how to mask the inner levels when simulating the outer domains. “Multi-zone” “Cyclic-zoom” masked the inner levels by freezing the hydrodynamic variables while evolving the magnetic fields within the mask region using inductive electric fields, preserving the divergence-free constraints on smaller scales through constraint transport [16, 17].

**[HYW: Temporal variability hierarchy.]** Despite the huge success of these novel methods, they could still suffer from the temporal variability problem.

**[HYW: Neural Operator]** In this paper, we start

**[HYW: Paper Structure.]** The structure of the paper

<sup>1</sup>  $\delta$  equal contribution

is as follows. [HYW: multiscal-NO?] In Section IV and V, we describe the numerical methods for direct simulations and algorithm of NO. In Section VII, we describe the problem setups and datasets used for training NOs. In Section VIII, we present the results: comparing the long-term roll-out of NOs and the direct simulations, and showing the large-scale simulations with NOs as the inner boundary condition. We then conclude in Section IX.

## II. DIFFICULT OF CAPTURING VARIABILITY IN MULTISCALE PROBLEMS

### III. OVERVIEW OF MULTISCALE-NO FRAMEWORK

#### A. Run Duration

#### IV. METHOD-SIMULATION

We use a performance portable version of Athena++ [18] based on Kokkos library [19]-AthenaK [20].

#### A. Magneto-hydrodynamics Simulations: Magnetized SCAF

The setup we use in this work is a magnetized version of SCAF [8], without cooling and heating terms. In this case, we solve the Newtonian magnetohydrodynamics equations in conservative form:

$$\frac{\partial \rho}{\partial t} + \nabla \cdot (\rho \mathbf{v}) = s_\rho, \quad (1)$$

$$\frac{\partial(\rho \mathbf{v})}{\partial t} + \nabla \cdot (\rho \mathbf{v} \mathbf{v} + P \mathbf{I} - \mathbf{B} \mathbf{B}) = \mathbf{s}_p - \rho \nabla \Phi, \quad (2)$$

$$\frac{\partial E}{\partial t} + \nabla \cdot [(E + P) \mathbf{v} - (\mathbf{B} \cdot \mathbf{v}) \mathbf{B}] = s_E - \rho \mathbf{v} \cdot \nabla \Phi, \quad (3)$$

$$\frac{\partial \mathbf{B}}{\partial t} - \nabla \times [\mathbf{v} \times \mathbf{B}] = 0, \quad (4)$$

where  $\rho : \mathbb{R}^3 \rightarrow \mathbb{R}$  is the gas density,  $\mathbf{v} : \mathbb{R}^3 \rightarrow \mathbb{R}^3$  is the velocity,  $P : \mathbb{R}^3 \rightarrow \mathbb{R}$  is the pressure,  $E = P/(\gamma-1) + \rho|\mathbf{v}|^2/2$  is the total energy density, and  $-\nabla \Phi$  is the gravitational acceleration due to the central accretor. The flow evolved following ideal gas law with adiabatic index  $\gamma = 5/3$ .

In code unit,  $GM = r_0 = \rho_0 = 1$ . The output quantities include  $(\rho, P, \mathbf{v} = (v_x, v_y, v_z), \mathbf{B} = (B_x, B_y, B_z))$ .

We use piecewise parabolic reconstruction [21], an HLLD Riemann solver [22], a constraint transport algorithm [17] for the divergence-free magnetic field evolution, and first-order flux correction [23].

## B. GRMHD Simulations

The conservative Valencia formulations for solving GRMHD equations with induction equation

$$\partial_t \mathbf{U} + \partial_i \mathbf{F} = \mathbf{S} \quad (5)$$

$$\partial_t(\sqrt{-g}B^i) + \partial_j(\sqrt{-g}(b^i u^j - b^j u^i)) = 0 \quad (6)$$

where the conserved variables, fluxes, and source terms associated with the connection are

$$\begin{aligned} \mathbf{U} &= \sqrt{-g} \begin{bmatrix} \rho u^t \\ T_i^t \\ T_t^t + \rho u^t \end{bmatrix}, \\ \mathbf{F} &= \sqrt{-g} \begin{bmatrix} \rho u^j \\ T_i^j \\ T_t^j + \rho u^j \end{bmatrix}, \\ \mathbf{S} &= \sqrt{-g} \begin{bmatrix} 0 \\ \frac{1}{2}(\partial_i g_{\alpha\beta})T^{\alpha\beta} \\ 0 \end{bmatrix} \end{aligned} \quad (7)$$

respectively, where the metric is  $\mathbf{g}$  and  $g = \det \mathbf{g}$ . The rest-mass density is  $\rho$ , the coordinate frame 4-velocity is  $u^\mu$  and the stress-energy tensor is

$$T^\mu{}_\nu = w u^\mu u_\nu - b^\mu b_\nu + (p_g + p_m) \delta^\mu_\nu \quad (8)$$

where the magnetic field is  $b^\mu$ , the magnetic pressure is  $p_m = b_\mu b^\mu/2$ , and the total enthalpy is  $w$ . The non-monopole constraint is preserved when evolving the 3-components  $B^i$  of the magnetic field:

$$\partial_j(\sqrt{-g}B^j) = 0 \quad (9)$$

where

$$b^t = u_i B^i \quad (10)$$

$$b^i = \frac{1}{u^t}(B^i + b^t u^i) \quad (11)$$

We solve the GRMHD equations in a Cartesian Kerr-Schild coordinate. We adopt piecewise parabolic spatial reconstruction, HLLC Riemann solver, RK2 time integrator, and first-order flux correction [23].

In all runs, we adopt  $G = M = \rho_0 = 1$

## V. METHOD-NO

### A. Learning

Define the semigroup  $\{S(h)\}_{h>0}$  as

$$\begin{aligned} S(h) : & (\rho(x, t), P(x, t), v(x, t)) \rightarrow \\ & (\rho(x, t+h), P(x, t+h), v(x, t+h)). \end{aligned} \quad (12)$$

Our target is to learn a neural surrogate  $G_\theta$  that approximates  $S(h)$  for a particular  $h$ .

Basic Method: Supervised Learning.

Use FNO as the ansatz of  $G_\theta$ . Train the FNO by fitting data (input-output pairs) from numerical solvers.

In this project, we employed LocalNO to better capture small-scale (high-frequency) information.

### 1. Problem-Specific Methods

1. Logarithm transform for density and energy.
2. Position information. The center of the blackhole, though only taking up a tiny portion of the domain, plays a vital role in the simulation. We notice that the standard approach to doing position embedding fails to achieve satisfactory performance. We divide the domain into 8 (?) regions determined by the distance from the center and apply one-hot embedding, namely the grid points in the  $i$ -th region is equipped with a feature vector  $e_i \in \mathbb{R}^8$ . Further, we reweight the loss function, replacing vanilla  $L^2$  norm  $\int |u(x) - v(x)|^2 dx$  with  $\int |u(x) - v(x)|^2 \lambda(x) dx$ , forcing the model to learn the center well at an early stage of the training.
3. Enforcing physical scaling relations. We know that several quantities (denoted by  $u$ ) approximately satisfy a scaling relation, i.e.,  $u(r)$  decays exponentially w.r.t.  $r$ , the distance to the blackhole center. To make training easier and more stable, the model is optimized to learn the residual.

$$\log(u(x)) = k|x| + G_\theta(\log(u(x))), \quad (13)$$

where  $k$  is estimated through the dataset. We enforce the model output to be smaller than a pre-assigned value  $C$  through a regularizer.

### B. Effective Conservation Law

We apply the angular-integrated conservation law for mass and angular momentum as loss functions. Even without reaching a quasi-steady state, the angular integrated continuity equation and momentum conservation equations should hold. *[But for now we abandon the terms associated with the time derivative, by assuming a quasi-steady state (including accretion and feedback) has been reached, then the mass accretion rate and the specific angular momentum transport along the radial direction should be constant.] [This assumption should hold as the domain/level of interest utilized for training has reached a quasi-steady state.]*

The integral form of continuity equation

$$\frac{\partial}{\partial t} \int_{r_i}^{r_{i+1}} \langle \rho \rangle_{\theta, \phi} dr + \langle \rho v_r \rangle_{\theta, \phi} \Big|_{r_i}^{r_{i+1}} = 0 \quad (14)$$

and the momentum conservation equation

$$\frac{\partial}{\partial t} \int_{r_i}^{r_{i+1}} \langle \rho v_\phi \rangle_{\theta, \phi} dr + \langle \rho v_r v_\phi - B_r B_\phi \rangle_{\theta, \phi} \Big|_{r_i}^{r_{i+1}} = 0 \quad (15)$$

Removing the time derivative terms, we can use the angular integrated values within each spherical shell to ensure

mass and angular momentum conservation:

$$\dot{M} = \langle \rho v_r \rangle_{\theta, \phi} \quad (16)$$

$$\dot{J} = \langle \rho v_r v_\phi - B_r B_\phi \rangle_{\theta, \phi} \quad (17)$$

energy flux and magnetic flux  
only train on primitive variables (not cons) for GRMHD  
time hierarchy

- interpolation: linear/parabolic (or subcycling)
- extrapolation: past time
- interpolation inside FNO  $\rightarrow$  enforce the semigroup
- 

### C. Single-level

### D. Two-level

### E. Nested two-level as multi-level cyclic-zoom

## VI. DIAGNOSTICS

### A. Hydrodynamics

### B. MHD

### C. GRMHD

For consistency, we apply the diagnostics same as the previous GRMHD simulation [14]. The relevant diagnostics include mass flux, magnetic field flux, energy flux, radial momentum flux, and angular momentum flux:

$$\dot{M} \equiv - \int_S \rho u^r \sqrt{-g} d\Omega, \quad (18)$$

$$\Phi_{\text{BH}} \equiv \sqrt{\pi} \int_S |B^r| \sqrt{-g} d\Omega, \quad (19)$$

$$\dot{E} \equiv \int_S T^r_t \sqrt{-g} d\Omega, \quad (20)$$

$$\dot{p}_r \equiv \int_S T^r_r \sqrt{-g} d\Omega, \quad (21)$$

$$\dot{L} \equiv \int_S T^r_\phi \sqrt{-g} d\Omega, \quad (22)$$

where  $S$  is the area,  $T^r_t = (\rho + u + p + b^2)u^r u_t - b^r b_t$ , and  $T^r_\phi = (\rho + u + p + b^2)u^r u_\phi - b^r b_\phi$ . Sometimes it is useful to separate the mass flux into inflow and outflow:

$$\dot{M} = - \underbrace{\int_{u^r < 0} \rho u^r \sqrt{-g} d\Omega}_{\dot{M}_{\text{in}}} - \underbrace{\int_{u^r > 0} \rho u^r \sqrt{-g} d\Omega}_{\dot{M}_{\text{out}}}. \quad (23)$$

The dimensionless magnetic flux parameter is defined by

$$\phi_{\text{BH}} \equiv \frac{\Phi_{\text{BH}}}{\sqrt{\dot{M}}}. \quad (24)$$

The energy flux  $\dot{E}$  includes the flux of rest-mass energy, so the “feedback” energy flux is  $\dot{M} - \dot{E}$ . The efficiency of feedback can thus be defined by

$$\eta \equiv \frac{\dot{M} - \dot{E}}{\dot{M}}. \quad (25)$$

The efficiency is positive (negative) when energy is transported outward (inward). We can further separate the feedback power into the hydrodynamic part and the electromagnetic (EM) part

$$\dot{E}_{\text{hydro}} = - \int_S [(\rho + u + p)u^r u_t + \rho u^r] \sqrt{-g} d\Omega, \quad (26)$$

$$\dot{E}_{\text{EM}} = - \int_S (b^2 u^r u_t - b^r b_t) \sqrt{-g} d\Omega, \quad (27)$$

## VII. PROBLEM SETUPS AND DATASETS

### A. Newtonian MHD from large-scale zoom-in

- floor and cap
- output frequency
- downsampled size/resolution

### B. GRMHD

The initial condition is a cloud of gas with constant mass density  $\rho = \rho_0$  and constant angular momentum. We cho

## VIII. RESULTS

## IX. DISCUSSION AND CONCLUSION

[HYW: Conclusions.] In this work, we present a method combining neural operator and direct numerical simulations for accretion and feedback problem, in both magnetohydrodynamic and general relativistic magneto-hydrodynamic simulations.

We demonstrate the validity of the method by training on MHD and GRMHD simulations of magnetized Bondi accretion onto a central black hole.

- (1)
- (2)
- (3)
- \* begin
- \* end

This is aimed to motivate the future development of machine-learning-based subgrid models in galactic and cosmological simulations, capturing both the statistically averaged mass and energy feedback information and the variability simultaneously.

[HYW: Future Prospective.] The method presented in this paper is a first step (two-level version) towards a multi-level cyclic-zoom/multi-zone neural operator framework for simulations around a central accretor.

## X. ACKNOWLEDGEMENT

The authors are grateful for discussions with Philip Hopkins, Yoonsoo Kim, Wenrui Xu, and Hengrui Zhu. HYW thanks Minghao Guo for discussions on a closely related project. ERM and HYW acknowledge support from the National Science Foundation through award NSF-AST2508940. Part of the simulations were performed on DOE OLCF Summit under allocation AST198. This research used resources of the Oak Ridge Leadership Computing Facility at the Oak Ridge National Laboratory, which is supported by the Office of Science of the U.S. Department of Energy under Contract No. DE-AC05-00OR22725. Part of this project was completed during the Caltech relativistic astrophysics summer school, which was supported by the National Science Foundation.

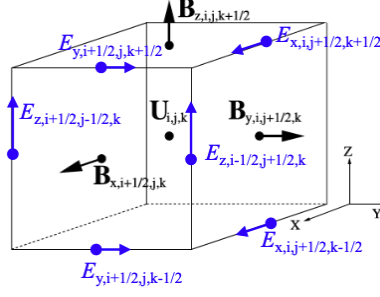


FIG. 1. Positions of hydrodynamic variables, magnetic fields, and electric fields. The hydrodynamic variables are at the body-center of each cell, while the electric fields and magnetic fields are at the face-centers and edge-centers.

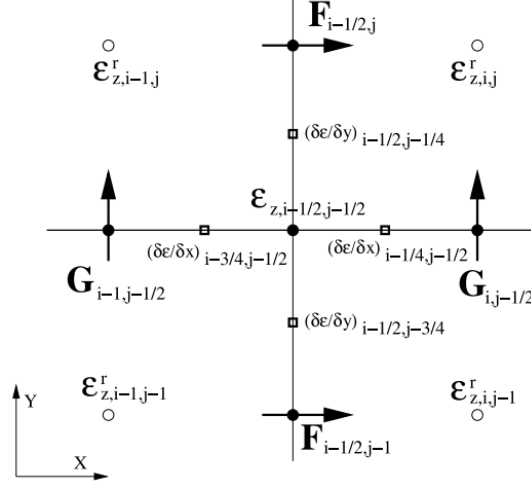


FIG. 2. [HYW: Adopting from Athena method paper-remake later] The schematic diagram of the x-y slice, in which shows the cell-centered reference state of EMF  $E_z^r$ , cell-cornered EMF  $E_z$  used for recovering the area-averaged magnetic field, and the fluxes of conserved variables in the x and y directions.

## Appendix A: Constraint Transport on the Boundary: NO as Riemann Solver

### 1. Review: Divergence-Free Magnetic Field and Constraint Transport

The magnetic fields are evolved via Stoke's law:

$$\frac{\partial}{\partial t} \int_S \mathbf{B} \cdot d\mathbf{S} = - \int_L \mathbf{E} \cdot d\mathbf{l}, \quad (\text{A1})$$

in the differential form :

$$\frac{\partial \mathbf{B}}{\partial t} + \nabla \times \mathbf{E} = 0, \quad (\text{A2})$$

where the electric field (electromotive force [EMF])  $\mathbf{E} = -\mathbf{v} \times \mathbf{B}$  in ideal MHD.

Constraint transport (CT) algorithm update the area-averaged magnetic fields using the line-averaged EMF at cell corners. First, we can separately define the face-centered, area-averaged magnetic field  $(B_x)_{i+1/2,j,k}$  and the edge-centered, line-averaged EMF  $(E_x)_{i,j+1/2,k-1/2}$  as follow (taking x-component as an example):

$$(B_x)_{i+1/2,j,k} = \frac{1}{\Delta y \Delta z} \int_S B_x(y, z) dy dz, \quad (\text{A3})$$

$$(E_x)_{i,j+1/2,k-1/2} = \frac{1}{\Delta x \Delta t} \int E_x(x) dx dt, \quad (\text{A4})$$

The magnetic field at the  $n + 1$  timestep is updated using the electro-magnetic forces accordingly

$$B_{x,i+1/2,j,k}^{n+1} = B_{x,i+1/2,j,k}^n - \frac{\Delta t}{\Delta y} \left( E_{z,i-1/2,j+1/2,k}^{n+1/2} - E_{z,i-1/2,j-1/2,k}^{n+1/2} \right) + \frac{\Delta t}{\Delta z} \left( E_{y,i-1/2,j,k+1/2}^{n+1/2} - E_{y,i-1/2,j,k-1/2}^{n+1/2} \right) \quad (\text{A5})$$

Then the divergence of magnetic field  $\nabla \cdot \mathbf{B}$  is preserved to machine accuracy

$$\nabla \cdot \mathbf{B} = \frac{B_{x,i+1/2,j,k} - B_{x,i-1/2,j,k}}{\Delta x} + \frac{B_{y,i,j+1/2,k} - B_{y,i,j-1/2,k}}{\Delta y} + \frac{B_{z,i,j,k+1/2} - B_{z,i,j,k-1/2}}{\Delta z} \quad (\text{A6})$$

## 2. Coupling NO with Constraint Transport

In **Athena++/K**, it is the Riemann solver that returns area-averaged electric fields at cell faces, while the CT requires the line-averaged EMF at cell corners to update the area-averaged magnetic fields, here this is achieved by [17, 24, 25]:

$$E_{z,i-1/2,j-1/2} = \frac{1}{4} (E_{z,i-1/2,j} + E_{z,i-1/2,j+1} + E_{z,i,j-1/2} + E_{z,i+1,j-1/2}) \quad (\text{A7})$$

$$+ \frac{\delta y}{8} \left[ \left( \frac{\partial E_z}{\partial y} \right)_{i-1/2,j-1/4} - \left( \frac{\partial E_z}{\partial y} \right)_{i-1/2,j-3/4} \right] \quad (\text{A8})$$

$$+ \frac{\delta x}{8} \left[ \left( \frac{\partial E_z}{\partial x} \right)_{i-1/4,j-1/2} - \left( \frac{\partial E_z}{\partial x} \right)_{i-3/4,j-1/2} \right], \quad (\text{A9})$$

where the derivatived of EMF on each cell face is computed from the upwinded contact mode from the Riemann solver, i.e., suppressing the  $j$  subscript,

$$\left( \frac{\partial E_z}{\partial y} \right)_{i-1/2} = \begin{cases} (\partial E_z / \partial y)_{i-1}, & \text{for } v_{x,i-1/2} > 0 \\ (\partial E_z / \partial y)_i, & \text{for } v_{x,i-1/2} < 0 \\ \frac{1}{2} \left[ \left( \frac{\partial E_z}{\partial y} \right)_{i-1} + \left( \frac{\partial E_z}{\partial y} \right)_i \right], & \text{otherwise,} \end{cases} \quad (\text{A10})$$

The cell-centered derivatives of EMF are calculated from the face-centered EMF (Godunov flux) and cell-centered reference EMF  $E_z^r$  (see Fig. 2):

$$\left( \frac{\partial E_z}{\partial y} \right)_{i,j-1/4} = 2 \left( \frac{E_{z,i,j}^r - E_{z,i,j-1/2}}{\delta y} \right), \quad (\text{A11})$$

For more details on how to compute the reference EMF in certain timestep [\[HYW: refine the description here\]](#), see [25].

Since the NO is trained to predict the cell-centered volume-averaged magnetic field, from Eq. A9 and A11, we replace the face-centered EMF from Riemann solver with that from NO prediction (using the )

## Appendix B: Global Angular Momentum Transport

### 1. Cylindrical Coordinate

In this section we want to briefly review the equations governing the transport of total angular momentum. We do so by starting out with the ideal MHD equations in cylindrical coordinates. Denoting  $R$  as the cylindrical radius and  $z$  as the height coordinate, the conserved angular momentum density  $j^2$  then given by

$$j = R^2 \rho v_\phi \quad (\text{B1})$$

<sup>2</sup> [The specific angular momentum is  $l = Rv_\phi$ . To have the conserved angular momentum in the radial direction, one need to do the integration along both azimuthal and vertical directions

$\int R d\phi \int dz \rho l = \int d\phi \int dz (R^2 \rho v_\phi)$ . So the conserved angular momentum current across different cylinders (having  $R$  constant) has the form of  $j = R^2 \rho v_\phi$ ]

The momentum equation then takes the form

$$\partial_t j + \partial_R (j v_R + R^2 B_R B_\phi) + \partial_\phi (j + R B_\phi B_\phi + R \bar{P}) + \partial_z (j v_z + R^2 B_z B_\phi) - R \rho \partial_\phi \Phi_g = 0. \quad (\text{B2})$$

In practice, we are mainly interested in the transport of angular momentum in radius  $R$  and height  $z$ , so we will average over the  $\phi$  direction. This is appropriate for both the outer and the individual minidisks. Defining the azimuthally averaged angular momentum density,

$$\langle j \rangle_\phi = \int_0^{2\pi} d\phi j \quad (\text{B3})$$

we obtain

$$\partial_t \langle j \rangle_\phi + \partial_R (\langle j v_R \rangle_\phi + R^2 \langle B_R B_\phi \rangle_\phi) + \partial_z (\langle j v_z \rangle_\phi + R^2 \langle B_z B_\phi \rangle_\phi) - R \langle \rho \partial_\phi \Phi_g \rangle_\phi = 0. \quad (\text{B4})$$

the components appearing as derivatives in  $\phi$  are canceled from the azimuthally periodic nature.

## 2. Spherical Coordinate

### a. Radial Angular Momentum Balance

Angular momentum flux advected along the disk can be calculated by doing the integration in the  $\phi$  and  $z$  directions. For convenience, in the following we will use the notation:

$$\begin{aligned} \langle Q \rangle_{\phi,z} (R) &= \int_0^{2\pi} d\phi' \int_{z_{\text{lower}}}^{z_{\text{upper}}} dz' \cdot Q(R, \phi', z') \\ \langle Q \rangle_R &= \int_0^R dR' \cdot Q(R') \\ \langle Q \rangle_t &= \int dt' \cdot Q(t') \end{aligned}$$

The momentum equation can be further modified as

$$\begin{aligned} \int dz [\partial_t \langle j \rangle_\phi] &= - \int dz \partial_R \langle j v_R \rangle_\phi - \int dz \partial_z \langle j v_z \rangle_\phi \\ &\quad - \int dz \partial_R (R^2 \langle B_R B_\phi \rangle_\phi) - \int dz \partial_z (R^2 \langle B_z B_\phi \rangle_\phi) - \int dz R \langle \rho \partial_\phi \Phi_g \rangle_\phi \\ \partial_t \langle j \rangle_{\phi,z} &= - \partial_R \langle j v_R \rangle_{\phi,z} - \langle j v_z \rangle_\phi \Big|_{z_{\text{lower}}}^{z_{\text{upper}}} \\ &\quad - \partial_R (R^2 \langle B_R B_\phi \rangle_{\phi,z}) - R^2 \langle B_z B_\phi \rangle_\phi \Big|_{z_{\text{lower}}}^{z_{\text{upper}}} - R \langle \rho \partial_\phi \Phi_g \rangle_{\phi,z} \end{aligned}$$

We can reformulate the radial balance into a more compact form:

$$\partial_t \left( \frac{dJ}{dR} \right) = \frac{\partial \dot{J}_{\text{adv},R}}{\partial R} + \frac{dT_{\text{adv},z}}{dR} + \frac{\partial \dot{J}_{\text{mag},R}}{\partial R} + \frac{dT_{\text{mag},z}}{dR} + \frac{dT_{\text{grav}}}{dR}$$

where we have defined

(1) radial dependence of total angular momentum

$$\frac{dJ}{dR} = - \langle j \rangle_{\phi,z}$$

(2) inward angular momentum flux from advection

$$\dot{J}_{\text{adv},R} = - \langle j v_R \rangle_{\phi,z}$$

(3) torque from vertical transport (wind)

$$\left\langle \frac{dT_{\text{adv},z}}{dR} \right\rangle_R = - \int dR' \langle j v_z \rangle_\phi \Big|_{z_{\text{lower}}}^{z_{\text{upper}}}$$

(4) inward angular momentum flux from magnetic transport in the radial

$$\dot{J}_{\text{mag},R} = - R^2 \langle B_R B_\phi \rangle_{\phi,z}$$

(5) magnetic torque per unit radius

$$\left\langle \frac{dT_{\text{mag},z}}{dR} \right\rangle_R = - \int dR' R'^2 \langle B_z B_\phi \rangle_\phi \Big|_{z_{\text{lower}}}^{z_{\text{upper}}}$$

(6) gravitational torque per unit radius

$$\left\langle \frac{dT_{\text{grav}}}{dR} \right\rangle_R = - \int dR' R' \langle \rho \partial_\phi \Phi_g \rangle_{\phi,z}$$

After we do the time averaging of the above equation and assume a steady state of accretion ( $\partial_t = 0$ ), the accretion disk reaches a steady state.

$$\frac{d \langle \dot{J} \rangle_t}{dR} = \frac{\partial}{\partial R} (\langle \dot{J}_{\text{adv},R} \rangle_t + \langle \dot{J}_{\text{mag},R} \rangle_t) + \left\langle \frac{dT_{\text{adv},z}}{dR} \right\rangle_t + \left\langle \frac{dT_{\text{mag},z}}{dR} \right\rangle_t + \left\langle \frac{dT_{\text{grav}}}{dR} \right\rangle_t$$

Integrating along the radial direction from the coordinate pole (which is also the location where different torque components vanishes due to  $R \equiv 0$ ), we have

$$\langle \dot{J}_B \rangle_t = \langle \dot{J} \rangle_t = \langle \dot{J}_{\text{adv},R} \rangle_t + \langle \dot{J}_{\text{mag},R} \rangle_t + \left\langle \frac{dT_{\text{adv},z}}{dR} \right\rangle_{R,t} + \left\langle \frac{dT_{\text{mag},z}}{dR} \right\rangle_{R,t} + \left\langle \frac{dT_{\text{grav}}}{dR} \right\rangle_{R,t}$$

where  $\dot{J}_B$  is the total torque exerted directly onto the binary.

### Appendix C: Pedagogical Introduction: GRMHD

[Valencia Formulations] The compact form of the relativistic MHD equations can be written in the conservative Valencia formulations.

$$\partial_t(\sqrt{\gamma}\mathbf{U}) + \partial_i(\sqrt{\gamma}\mathbf{F}^i) = \sqrt{\gamma}\mathbf{S} \quad (\text{C1})$$

where  $\mathbf{U}$  is the conserved variables,  $\mathbf{F}^i$  is the fluxes, and  $\mathbf{S}$  is the source terms.

The state vectors  $\mathbf{U}$ , flux vectors  $\mathbf{F}^i$ , and source terms  $\mathbf{S}$  have the following form:

$$\mathbf{U} = \begin{pmatrix} D \\ S_j \\ \mathcal{U} \\ B^j \end{pmatrix}, \quad \mathbf{F}^i = \begin{pmatrix} D\mathcal{V}^i \\ \alpha W_j^i - \beta^i S_j \\ \alpha S^i - \beta^i \mathcal{U} \\ B^j \mathcal{Y}^i - B^i \mathcal{V}^j \end{pmatrix}, \quad (\text{C2})$$

$$\mathbf{S} = \begin{pmatrix} 0 \\ \frac{1}{2}\alpha W^{ik}\partial_j\gamma_{ik} + S_i\partial_j\beta^i - \mathcal{U}\partial_j\alpha \\ \frac{1}{2}W^{ik}\beta^j\partial_j\gamma_{ik} + W_i^j\partial_j\beta^i - S^j\partial_j\alpha \\ 0 \end{pmatrix}. \quad (\text{C3})$$

$$\nabla_\mu \tilde{J}^\mu = \nabla_\mu \rho u^\mu = 0, \quad (\text{C4})$$

$$\nabla_\mu T^{\mu\nu} = 0, \quad (\text{C5})$$

We can start from the covariant continuity equation (C4), which can be written as

$$\begin{aligned} \nabla_\mu(\rho u^\mu) &= \frac{1}{\sqrt{-g}}\partial_\mu(\sqrt{-g}\rho u^\mu) \\ &= \frac{1}{\sqrt{-g}}[\partial_t(\sqrt{-g}\rho u^t) + \partial_i(\sqrt{-g}\rho u^i)] = 0, \end{aligned} \quad (\text{C6})$$

- 
- [1] L. G. Fishbone and V. Moncrief, Relativistic fluid disks in orbit around Kerr black holes., *Astrophys. J.* **207**, 962 (1976).
  - [2] H. Bondi, On spherically symmetrical accretion, *Mon. Not. Roy. Astron. Soc.* **112**, 195 (1952).
  - [3] A. Lalakos, O. Gottlieb, N. Kaaz, K. Chatterjee, M. Liska, I. M. Christie, A. Tchekhovskoy, I. Zhuravleva, and E. Nokhrina, Bridging the Bondi and Event Horizon Scales: 3D GRMHD Simulations Reveal X-shaped Radio Galaxy Morphology, *Astrophys. J. Lett.* **936**, L5 (2022), arXiv:2202.08281 [astro-ph.HE].
  - [4] A. Lalakos, A. Tchekhovskoy, O. Bromberg, O. Gottlieb, J. Jacquemin-Ide, M. Liska, and H. Zhang, Jets with a Twist: The Emergence of FR0 Jets in a 3D GRMHD Simulation of Zero-angular-momentum Black Hole Accretion, *Astrophys. J.* **964**, 79 (2024), arXiv:2310.11487 [astro-ph.HE].



- [5] H. R. O. S., M. A. Moscibrodzka, and O. Porth, General relativistic hydrodynamic simulations of perturbed transonic accretion, *Astron. Astrophys.* **678**, A141 (2023), arXiv:2301.12020 [astro-ph.HE].
- [6] A. Lalakos, A. Tchekhovskoy, E. R. Most, B. Ripperda, K. Chatterjee, and M. Liska, Universal Radial Scaling of Large-Scale Black Hole Accretion for Magnetically Arrested And Rocking Accretion Disks, arXiv e-prints , arXiv:2505.23888 (2025), arXiv:2505.23888 [astro-ph.HE].
- [7] M. Guo, J. M. Stone, C.-G. Kim, and E. Quataert, Toward Horizon-scale Accretion onto Supermassive Black Holes in Elliptical Galaxies, *Astrophys. J.* **946**, 26 (2023), arXiv:2211.05131 [astro-ph.HE].
- [8] M. Guo, J. M. Stone, E. Quataert, and C.-G. Kim, Magnetized Accretion onto and Feedback from Supermassive Black Holes in Elliptical Galaxies, arXiv e-prints , arXiv:2405.11711 (2024), arXiv:2405.11711 [astro-ph.HE].
- [9] P. F. Hopkins, M. Y. Grudic, K.-Y. Su, S. Wellons, D. Angles-Alcazar, U. P. Steinwandel, D. Guszejnov, N. Murray, C.-A. Faucher-Giguere, E. Quataert, and D. Keres, FORGE'd in FIRE: Resolving the End of Star Formation and Structure of AGN Accretion Disks from Cosmological Initial Conditions, *The Open Journal of Astrophysics* **7**, 18 (2024), arXiv:2309.13115 [astro-ph.GA].
- [10] P. F. Hopkins, J. Squire, K.-Y. Su, U. P. Steinwandel, K. Kremer, Y. Shi, M. Y. Grudic, S. Wellons, C.-A. Faucher-Giguere, D. Angles-Alcazar, N. Murray, and E. Quataert, FORGE'd in FIRE II: The Formation of Magnetically-Dominated Quasar Accretion Disks from Cosmological Initial Conditions, *The Open Journal of Astrophysics* **7**, 19 (2024), arXiv:2310.04506 [astro-ph.HE].
- [11] H. Cho, B. S. Prather, R. Narayan, P. Natarajan, K.-Y. Su, A. Ricarte, and K. Chatterjee, Bridging Scales in Black Hole Accretion and Feedback: Magnetized Bondi Accretion in 3D GRMHD, *Astrophys. J. Lett.* **959**, L22 (2023), arXiv:2310.19135 [astro-ph.HE].
- [12] H. Cho, B. S. Prather, K.-Y. Su, R. Narayan, and P. Natarajan, Multizone Modeling of Black Hole Accretion and Feedback in 3D GRMHD: Bridging Vast Spatial and Temporal Scales, *Astrophys. J.* **977**, 200 (2024), arXiv:2405.13887 [astro-ph.HE].
- [13] H. Cho, B. S. Prather, R. Narayan, K.-Y. Su, and P. Natarajan, Bridging Scales in Black Hole Accretion and Feedback: Relativistic Jet linking the Horizon to the Host Galaxy, arxiv (2025), arXiv:2507.17818 [astro-ph.HE].
- [14] M. Guo, J. M. Stone, E. Quataert, and V. Springel, Cyclic Zoom: Multi-scale GRMHD Modeling of Black Hole Accretion and Feedback, arxiv (2025), arXiv:2504.16802 [astro-ph.HE].
- [15] F. Yuan, M. Wu, and D. Bu, Numerical Simulation of Hot Accretion Flows. I. A Large Radial Dynamical Range and the Density Profile of Accretion Flow, *ApJ* **761**, 129 (2012), arXiv:1206.4157 [astro-ph.HE].
- [16] D. S. Balsara and D. S. Spicer, A Staggered Mesh Algorithm Using High Order Godunov Fluxes to Ensure Solenoidal Magnetic Fields in Magnetohydrodynamic Simulations, *Journal of Computational Physics* **149**, 270 (1999).
- [17] T. A. Gardiner and J. M. Stone, An unsplit Godunov method for ideal MHD via constrained transport in three dimensions, *Journal of Computational Physics* **227**, 4123 (2008), arXiv:0712.2634 [astro-ph].
- [18] J. M. Stone, K. Tomida, C. J. White, and K. G. Felker, The Athena++ Adaptive Mesh Refinement Framework: Design and Magnetohydrodynamic Solvers, *Astrophys. J.s* **249**, 4 (2020), arXiv:2005.06651 [astro-ph.IM].
- [19] C. Trott, L. Berger-Vergiat, D. Poliakoff, S. Rajamanickam, D. Lebrun-Grandie, J. Madsen, N. Al Awar, M. Gligoric, G. Shipman, and G. Womeldorff, The Kokkos EcoSystem: Comprehensive Performance Portability for High Performance Computing, *Computing in Science and Engineering* **23**, 10 (2021).
- [20] J. M. Stone, P. D. Mullen, D. Fielding, P. Grete, M. Guo, P. Kempster, E. R. Most, C. J. White, and G. N. Wong, AthenaK: A Performance-Portable Version of the Athena++ AMR Framework, arXiv e-prints , arXiv:2409.16053 (2024), arXiv:2409.16053 [astro-ph.IM].
- [21] P. Colella and P. R. Woodward, The Piecewise Parabolic Method (PPM) for Gas-Dynamical Simulations, *Journal of Computational Physics* **54**, 174 (1984).
- [22] T. Miyoshi and K. Kusano, A multi-state HLL approximate Riemann solver for ideal magnetohydrodynamics, *Journal of Computational Physics* **208**, 315 (2005).
- [23] M. N. Lemaster and J. M. Stone, Dissipation and Heating in Supersonic Hydrodynamic and MHD Turbulence, *Astrophys. J.* **691**, 1092 (2009), arXiv:0809.4005 [astro-ph].
- [24] T. A. Gardiner and J. M. Stone, An unsplit Godunov method for ideal MHD via constrained transport, *Journal of Computational Physics* **205**, 509 (2005), arXiv:astro-ph/0501557 [astro-ph].
- [25] J. M. Stone, T. A. Gardiner, P. Teuben, J. F. Hawley, and J. B. Simon, Athena: A New Code for Astrophysical MHD, *Astrophys. J. Suppl.* **178**, 137 (2008), arXiv:0804.0402 [astro-ph].